J. Phys. B: At. Mol. Opt. Phys. 24 (1991) 4025-4048. Printed in the UK

State-selective electron capture in collisions of He^{2+} with H

R Hoekstra†‡, F J de Heer‡ and R. Morgenstern†

† Kernfysisch Versneller Instituut, Zernikelaan 25, 9747 AA Groningen, The Netherlands
‡ FOM-Institute for Atomic and Molecular Physics, PO Box 41883, 1009 DB Amsterdam, The Netherlands

Received 24 April 1991, in final form 18 June 1991

Abstract. Charge transfer into $He^+(nl)$ states ($n < 5$) in collisions (2-13 keV amu^{-1}) of He^{2+} on atomic hydrogen has been studied by means of photon emission spectroscopy. State selective electron capture cross sections into the degenerate $He^+(4l)$ states have been determined by deconvoluting the intensity distribution of the He II ($n = 4 \rightarrow n = 3$) emission along the total ion-beam path inside the collision chamber. They are compared with theoretical results, especially with the large-basis set extended atomic orbital calculations of Fritsch. Generally good agreement with these extended calculations is found. However, the structures in the theoretical cross sections for capture into the non-dominantly populated $n = 4$ states are not observed experimentally.

1. Introduction

Electron capture processes in collisions of bare ions with atomic hydrogen are of fundamental interest (see e.g. the review by Janev and Winter 1985) and play an important role in the energy balance and the diagnostics of fusion plasmas, e.g. in connection with the injection of atomic hydrogen beams (Fonck *et al* 1984, Boileau *et al* 1989). Of the asymmetric bare ion-atomic-hydrogen collisions systems the simplest one is

$$He^{2+} + H \rightarrow He^+(nl) + H^+ \tag{1}$$

and so this system has been studied extensively both theoretically and experimentally. In the energy range of 1-15 keV amu^{-1} the results of the different theoretical methods—molecular orbital (MO) calculations by Winter and Hatton (1980), Kimura and Thorson (1981) and Errea *et al* (1987) and atomic orbital (AO) calculations by Bransden *et al* (1983), Winter (1988), Fritsch (1988) and Shingal and Lin (1989)—are in very good agreement with each other as far as total electron capture and capture into the dominant channel, $He^+(2p)$, is concerned.

Total charge transfer cross sections were first measured by Fite *et al* (1962) and later on by Shah and Gilbody (1974, 1978), Bayfield and Khayrallah (1975) and Nutt *et al* (1978). The measurements of Shah and Gilbody (1978) and Nutt *et al* (1978), which are believed to be the most accurate, are in excellent agreement with the theoretical results. However there is a long-standing discrepancy between measured (Shah and Gilbody 1978, Bayfield and Khayrallah 1975) and calculated cross sections for electron capture into $He^+(2s)$. Capture into $He^+(2s)$ accounts for approximately 20% of the total charge transfer cross section. The remaining and largest fraction is almost entirely due to capture into $He^+(2p)$. In the energy range of 1-10 keV amu^{-1}

0953-4075/91/184025+24$03.50 © 1991 IOP Publishing Ltd

the cross sections, $\sigma(2p)$, determined by Čirič *et al* (1985, 1988) were found to be in good agreement with theory.

Although capture into $n = 2$ accounts for more than 90% of the total one-electron capture cross section, cross sections for capture into states with $n \geq 3$ are of great importance, namely on the one hand for testing the reliability of theoretical predictions and on the other hand for future plasma diagnostics (Fonck *et al* 1984, Boileau *et al* 1989). The latter results from the fact that the detection of $\Delta n = 1$ transitions between high-n states, yielding light in the visible spectral region, can be done with radiation resistant fibre optical connections between spectrometers and fusion reactor. Now for the first time we have succeeded in measuring all contributions of different l states included in such a $\Delta n = 1$ transition, namely the $4l$ contributions to the He II ($n = 4 \rightarrow n = 3$) transition. The previously measured emission cross sections for the He II ($n = 4 \rightarrow n = 3$) transition (Čirič *et al* 1988) could not be used directly for plasma diagnostics since in a large tokamak the l states within one high-n shell are mixed (Fonck *et al* 1984, Boileau *et al* 1989). So experimental determination of the electron capture cross sections of the separate l states is needed.

By means of VUV photon emission spectroscopy we have measured the He II Lyman series ($np \rightarrow 1s$) with $n < 5$. The He II ($4p \rightarrow 1s$) transition gives direct information on the $He^+(4p)$ population. The 4s, 4d and 4f populations have to be deduced from the He II ($n = 4 \rightarrow n = 3$) transition. The spatial deconvolution technique used to determine these $4l$ cross sections will be described in section 2.2. Since we have also measured the He II ($n = 3 \rightarrow n = 2$) line emission we get an almost complete picture of state-selective charge transfer in collisions of He^{2+} with atomic hydrogen, especially in combination with the results of large-basis set atomic-orbital calculations (Fritsch 1988). The results of these calculations will be presented in tabulated form in section 3. In sections 3.1–3.3 our experimental and theoretical data will be compared with each other and with all the other available information on the He^{2+}–H system.

2. Experiment

2.1. Experimental set-up

The experimental set-up, schematically shown in figure 1, will be described only briefly, for details see Čirič *et al* (1985) and Hoekstra (1990). The He^{2+} ions have been produced with the electron cyclotron resonance (ECR) ion source of the MINIMAFIOS type (Geller and Jacquot 1982) installed at the KVI Groningen (Drentje 1985). In the set-up the ions cross a partly dissociated hydrogen beam produced by means of a Slevin-type 27 MHz radio-frequency source (Slevin and Stirling 1981). The absolute density profiles of the atomic and molecular components of the target beam were determined by observation of electron impact induced atomic (Balmer-β) and molecular radiation (Čirič *et al* 1985). The radiation was observed with a monochromator for visible light (300–600 nm) equipped with an imaging lens system which enables the detection of light along the ion beam. In the centre of the beam the effective density fraction of atomic hydrogen was found to be 75%. The He II ($n = 4 \rightarrow n = 3$) line emission at 468.6 nm has been observed perpendicular to the ion beam with the above mentioned spectrometer for visible light. The He II ($np \rightarrow 1s$) Lyman emission in the VUV (cf figure 2) has been detected with a VUV spectrometer. The latter spectrometer has been tilted 45° to avoid instrumental polarization effects (appendix A). This VUV monochromator

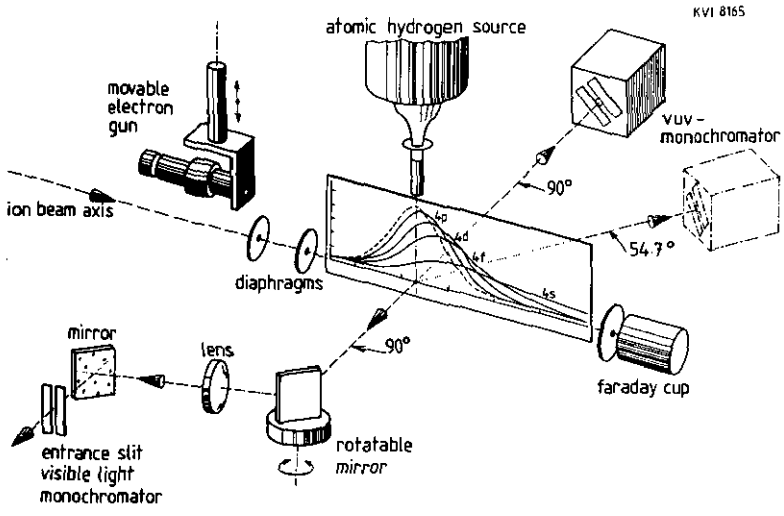

Figure 1. Schematic view of the experimental set-up. Typical spatial emission profiles of light resulting from the decay of the $He^{+}(4l)$ states are included. The target density profile is indicated by the broken curve.

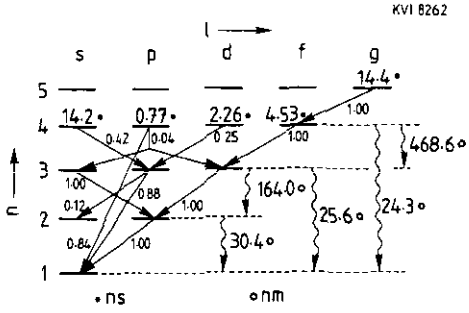

Figure 2. Energy level scheme of He II. The relevant transitions (wavelengths in nm) are shown together with the branching ratios and the lifetimes (in ns) of the $4l$ and 5g states.

is equipped with a position sensitive microchannel plate detector, which enables simultaneous detection of the He II Lyman lines. To measure the He II ($n = 3 \rightarrow n = 2$) transition at 164 nm the VUV monochromator has been replaced by a modified Seya-Namioka-type monochromator supplied with a solar blind photomultiplier. This photon detection system was not only tilted 45° but also positioned under the magic angle of 54.7° with respect to the ion beam (cf figure 1) to cancel all possible polarization effects (see appendix A). It should be noted that measurements of the above mentioned emission lines have been performed not only on the mixed H/H_2 target but also on a pure H_2 target, the latter being done to be able to subtract the H_2 contribution from the mixed target measurements.

2.2. Determination of contributions from degenerate states

To deduce the separate contributions of the $4l$ states to the He II ($n = 4 \rightarrow n = 3$) emission we have exploited the fact that the lifetimes of the states are different. Figure 2 shows the energy level scheme of He II together with the lifetimes and the branching ratios

of the states relevant for our experiment. Radiation from short-lived levels, e.g. 4p, is mainly concentrated on the target area, whereas radiation from long-lived states, e.g. 4s, is still emitted downstream from the collision centre. Therefore the measurement of emission profiles along the beam axis gives information on the l state populations. This method, often used in collision experiments on static targets (gas cell and beam–foil experiments) has only once been used in combination with a beam target, namely to measure capture into H($3l$) states in H^+–Li collisions (Aumayr *et al* 1984). The case of He^{2+} colliding on atomic hydrogen is more intricate since (i) more l states have to be included, (ii) the lifetimes of the states are closer to each other, (iii) the target has two components, H and H_2.

As mentioned above the spatial deconvolution method (for a detailed description, see Aumayr *et al* 1984) is based on the fact that the lifetimes of the upper levels are different, for the $He^+(4l)$ levels they vary from 0.77 (4p) to 14.2 ns (4s), see figure 2. Since the He^+ ion is hydrogen-like, the lifetimes are known accurately. Associated with the lifetimes are typical decay lengths $v \times \tau_{4l}$ (v the velocity of the ions and τ_{4l} the lifetimes of the $4l$ states). At a typical impact velocity of 0.5 au this length is 0.8 and 15 mm for 4p and 4s respectively. Therefore the radiation of the 4p level is emitted close to the collision centre whereas light from the 4s level may still be emitted further downstream the ion beam. Typical emission profiles are shown in figure 1 with respect to the dimensions of the experimental set-up.

Neglecting cascades the emission profiles, P_{4l} are described by

$$P_{4l}(z) = \frac{1}{v\tau_{4l}} \int_0^z T(z') \exp[-(z-z')/v\tau_{4l}] \, dz' \tag{2}$$

with v and τ_{4l} defined as before, z the position along the beam axis and $T(z)$ the target density profile. The target profiles have been measured by 400 eV electron impact excitation of Balmer-β emission (Čirič *et al* 1985, Hoekstra 1990). The shape of the profiles was checked before and after each measurement by using the primary He^{2+} beam to excite the target and measuring the resulting emission along the ion beam. At a certain position along the ion beam axis the measured He II ($n=4 \rightarrow n=4$) signal, $S(z)$, is equal to

$$S(z) = K \sum_l \beta(4l \rightarrow 3) P_{4l}(z) \sigma(4l) \tag{3}$$

with K an absolute calibration constant, $\beta(4l \rightarrow 3)$ the branching ratio for transitions to $n=3$ and $\sigma(4l)$ the electron capture cross sections. The signals have been measured at 25 to 30 positions along the beam axis, so it is possible to deduce the cross sections from a standard weighted least squares fit (Mathews and Walker 1970). To increase the accuracy of results of this fitting procedure the contribution of the 4p, which is relatively small due to the small branching ratio (see figure 2) has first been subtracted from the signals. As mentioned before the $\sigma(4p)$ can be determined directly from the He II ($4p \rightarrow 1s$) transition.

Figure 3(a) shows on an absolute scale the emission profiles for 5 keV amu^{-1} He^{2+} colliding on atomic hydrogen. It can be seen that the measurement is well described by the fit. Since at this impact energy the results differ from theory (as will be shown in section 3.3), figure 3(b) shows a convolution of the theoretical results in order to demonstrate that the theoretical prediction is not another solution for the fit. Scaling of the convolution to the maximum of the emission profile shows that downstream the ion beam axis the theoretical profile decreases somewhat stronger than the observed emission profile.

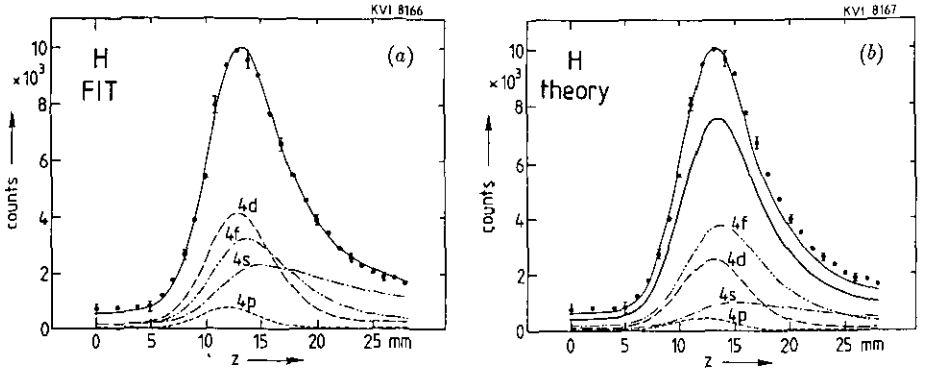

Figure 3. (*a*) Spatial He II ($n=4\rightarrow n=3$) emission profile resulting from 5 keV amu^{-1} He^{2+} colliding on H. The figure shows also the results of the deconvolution. (*b*) Convolution of the AO results at 5 keV amu^{-1} (table 4). The figure includes the contributions of the *different l levels* and their sum (thick full curve). The thin full curve is the result of scaling the summed values to the maximum of the emission profile.

2.3. Experimental results

The experimental results for the He II ($np\rightarrow 1s$), the He II ($n=3\rightarrow n=2$) and the He II ($n=4\rightarrow n=3$) transitions together with their relative errors are given in tables 1, 2 and 3 respectively. These tables include only the results for collisions on atomic hydrogen. The complementary data for collisions on molecular hydrogen will be presented in a subsequent paper (Hoekstra *et al* 1991) from now on referred to as II. Aside of the general relative and absolute errors, here we will discuss potential sources of errors like polarization, electric fields and the possible presence of metastable H(2s) in the target beam, which have not been treated fully in previous publications.

Table 1. Emission cross sections for the He II ($np\rightarrow 1s$) transitions resulting from He^{2+}–H collisions. The absolute systematic error is 15%, 18% and 20% for respectively $2p\rightarrow 1s$, $3p\rightarrow 1s$ and $4p\rightarrow 1s$.

	$2p\rightarrow 1s$ (Å^2)		$3p\rightarrow 1s$ (10^{-1} Å^2)		$4p\rightarrow 1s$ (10^{-2} Å^2)	
E (keV amu^{-1})	σ_{em}	$\Delta\sigma_{rel}$	σ_{em}	$\Delta\sigma_{rel}$	σ_{em}	$\Delta\sigma_{rel}$
13	10.0	0.5	3.9	0.2	7.0	0.7
12	10.9	0.5	3.5	0.2	6.5	0.6
11	10.9	0.5	3.1	0.2	5.6	0.6
10	11.0	0.5	3.2	0.2	5.0	0.5
9	10.9	0.5	3.1	0.2	4.5	0.5
8	10.8	0.5	3.0	0.2	4.6	0.5
7	10.2	0.5	3.1	0.2	4.1	0.5
6	9.5	0.5	3.0	0.2	3.5	0.4
5	9.4	0.5	2.9	0.2	2.7	0.4
4	8.3	0.4	2.5	0.2	1.8	0.3
3.5	7.4	0.4	2.2	0.2	1.3	0.3
3	6.8	0.4	2.0	0.18	1.2	0.3
2.5	5.8	0.3	1.65	0.15	0.6	0.3
2	4.3	0.3	1.08	0.12		

Table 2. He^{2+}–H: emission cross sections for the He II ($n=3\rightarrow n=2$) line in 10^{-17} cm^2. the absolute systematic error is 30%.

	$n=3\rightarrow n=2$			$n=3\rightarrow n=2$	
E (keV amu^{-1})	σ_{em}	$\Delta\sigma_{rel}$	E (keV amu^{-1})	σ_{em}	$\Delta\sigma_{rel}$
13	5.0	0.5	5.5	3.3	0.4
12	5.0	0.5	5	3.5	0.4
11	5.5	0.5	4.5	3.1	0.3
10	5.5	0.5	4	3.1	0.3
9	5.1	0.5	3.5	2.7	0.3
8	4.6	0.4	3	2.2	0.3
7	4.4	0.4	2.5	1.8	0.3
6	3.7	0.4	2	1.5	0.3

Table 3. He^{2+}–H: emission cross sections for the He II ($n=4\rightarrow n=3$) line and capture cross sections for 4s, 4d and 4f (in 10^{-18} cm^2). The 4s results include cascade contributions from 5g, see text. Absolute errors are 20%.

	$4\rightarrow 3$		4s		4d		4f	
E (keV amu^{-1})	σ	$\Delta\sigma_{rel}$	σ	$\Delta\sigma_{rel}$	σ	$\Delta\sigma_{rel}$	σ	$\Delta\sigma_{rel}$
13	6.8	0.6	3.1	0.5	4.7	0.9	4.0	0.8
12	6.8	0.6	3.3	0.6	4.7	0.9	3.9	0.75
11	6.5	0.6	3.1	0.5	4.7	0.9	3.7	0.6
10	6.1	0.55	3.2	0.6	5.5	1.0	3.1	0.55
9	5.8	0.5	4.3	0.8	3.9	0.8	2.8	0.55
8	5.3	0.5	3.4	0.6	4.8	0.9	2.5	0.5
7	4.2	0.4	2.7	0.5	4.1	0.8	1.9	0.4
6	3.8	0.35	1.6	0.4	4.2	0.8	1.8	0.4
5	2.7	0.3	1.6	0.4	3.1	0.6	1.1	0.3
4	2.0	0.3	1.2	0.25	2.1	0.5	0.9	0.25
3.5	2.0	0.3	1.3	0.3	2.5	0.5	0.7	0.2
3	1.85	0.3	0.86	0.2	2.0	0.5	0.95	0.25
2.5	1.5	0.3	0.6	0.15	1.35	0.4	0.6	0.2
2	1.3	0.3						

2.3.1. Relative errors. The relative errors in the emission cross sections are the quadratical sum of the statistical error at 90% confidence level and a target density uncertainty (estimated to be 5%) due to possible fluctuations in the overlap of the ion and target beams and in the dissociation degree. The estimation of 5% is based on the following experimental checks: (i) measurements of the He II ($2p\rightarrow 1s$) line emission on a static and on a beam target of molecular hydrogen. Within the experimental error bars we did not find a change in the effective target overlaps at different impact energies; (ii) measurements (at least twice a day) of the stability of the atomic hydrogen fraction of the partly dissociated hydrogen target. The target was found to be stable within 3%.

For the $\sigma(4l)$ capture cross sections deduced from spatial He II ($n=4\rightarrow n=3$) emission profiles the main contribution to the relative error is related to the deconvolution method. The errors in the cpature cross sections are deduced from changes in the cross sections due to variations (within the experimental error bars) in the target

profiles. The errors found from the least squares fit (the diagonal elements of the inverted least squares matrix) are much smaller than the ones due to the above mentioned uncertainties in the target profiles. It should be noted that the scatter in $\sigma(4l)$ for collisions on molecular hydrogen (see (II)) does not significantly influence the results presented here for atomic hydrogen (there is no complete dissociation and hence the contribution due to collisions on H_2 has to be subtracted) since (i) the deconvolution results describe very well the emission profiles resulting from collisions with a pure molecular hydrogen target and (ii) the molecular hydrogen target profiles are almost equal in shape for a pure and a partly dissociated target.

2.3.2. Polarization effects. Polarization of the emitted radiation may influence the cross sections determined from measured photon intensities. This can be avoided by tilting the spectrometers 45° and by observing the photon emission under 54.7° (magic angle) with the ion beam axis (appendix A). Only the measurements of the He II ($n=3\rightarrow n=2$) emission have been performed under these experimental conditions.

The monochromator used to measure the He II ($np\rightarrow 1s$) radiation has been tilted 45°, however for historical reasons it has been positioned perpendicular to the ion beam. Therefore the Lyman data are influenced by an anisotropic angular distribution of the photon emission. The correction factor for the anisotropy can vary between 0.86 and 1.09 (appendix A). Therefore the error due to neglecting polarization effects can range from −14% to 9%. This error has not been included in the relative errors, because it is expected to be much smaller. This expectation is based on the theoretical results of Winter and Hatton (1980), Kimura and Thorson (1981), Bransden and Noble (1981) and Fritsch (1988). Applying the formulae given in appendix A we have calculated from the theoretical $He^+(2pm)$ cross sections an anisotropy correction factor for the He II ($2p\rightarrow 1s$) transition which is almost constant and equal to 0.96 ± 0.01 over the whole energy range of 2–13 keV amu^{-1}. Assuming this value to be correct, our experimental results would be too large by approximately 4%. At 3, 5 and 8 keV amu^{-1} we have tried to check this by measuring the He II ($2p\rightarrow 1s$) emission cross sections also at the magic angle of 54.7°. The emission cross sections at 54.7° were indeed ~5% smaller than the ones at 90°, which is in accordance with the theoretical polarization factor of 0.96. However, this experimental test is not totally conclusive, because the measurements at 90° and 54.7° have an intrinsic error of ~5% each. For the He II ($3p\rightarrow 1s$) and especially the He II ($4p\rightarrow 1s$) the errors due to the counting statistics are that large that the errors due to polarization effects are negligible. Finally it should be mentioned that in section 4 the results will be compared with both uncorrected and polarization corrected theoretical results.

The photons of the He II ($n=4\rightarrow n=3$) transitions have been observed perpendicular to the ion beam with an untilted spectrometer to allow for scanning along the ion beam axis. Fortunately at the wavelength of this transition, 468.6 nm, the effect of the anisotropy and the instrumental sensitivity are opposite. This results in a total correction factor of one, with a possible maximum deviation smaller than 5% (see appendix A).

2.3.3. Electric fields. Because of the (quasi-) degeneracy of the excited states of the hydrogenic He^+ ion a small electric field will already have a significant effect on the wavefunctions describing the system. This Stark mixing (for details see appendix B) changes branching ratios and lifetimes. For example at an electric field of only 4 V cm^{-1} the lifetime of the 4f($j=\frac{5}{2}$ and $m_j=\frac{5}{2}$) state and its branching ratio for decay to $n=3$

decrease some 15% (appendix B). Since the H source is completely shielded with copper, which prevents RF power leaking into the collision chamber and charging up the nozzle, only two electric field components have to be considered. One is caused by the space charge of the ion beam and the other is induced by the ion traversing the magnetic field present.

Assuming an axially symmetric ion beam with a uniform charge density (the collimating diaphragms are much smaller than the diameter of the incident ion beam) we obtain the following equation for the electric field $F(r)$ in $V\,m^{-1}$ at a distance r from the ion beam axis

$$F(r)=\frac{rI}{2\pi\varepsilon_0 r_0^2 v} \tag{4}$$

with r_0 the radius of the beam in m, I the ion beam current in A and v the velocity of the ions in $m\,s^{-1}$. The electric field due to the magnetic field is

$$\boldsymbol{F}=\boldsymbol{v}\times\boldsymbol{B} \tag{5}$$

with $\boldsymbol{B}$ in T. The magnetic field is about 2.7×10^{-4} T (mainly due to the cyclotron installed at the KVI) and is directed perpendicular to the ion beam direction. Both contributions to the electric field are shown in figure 4. This figure shows clearly that the electric field due to the magnetic field can be large enough to (partly) mix some of the $4l$ states. Therefore we have compensated the magnetic field by means of two sets of Helmholtz coils (not shown in figure 1) assuring that the magnetic field perpendicular to the ion beam direction is everywhere smaller than 1×10^{-5} T. So its contribution to the electric field decreases by a factor of about 25 and is always smaller than $0.2\,V\,cm^{-1}$. Thus the total electric field does not exceed $0.5\,V\,cm^{-1}$. Such a field is small enough to neglect effects due to Stark mixing (cf appendix B).

2.3.4. Metastable H(2s) in the target. Even a small fraction (roughly 10^{-4}) of metastables in the target beam would severely influence the experimental results for $\sigma(4l)$. This can be seen from the fact that charge transfer in collisions of He^{2+} with metastable H(2s) populates dominantly the $He^{+}(n=4)$ level with a cross section, $\sigma(n=4)$, of approximately $10^{-14}\,cm^2$ (Blanco *et al* 1987), whereas for collisions with ground-state

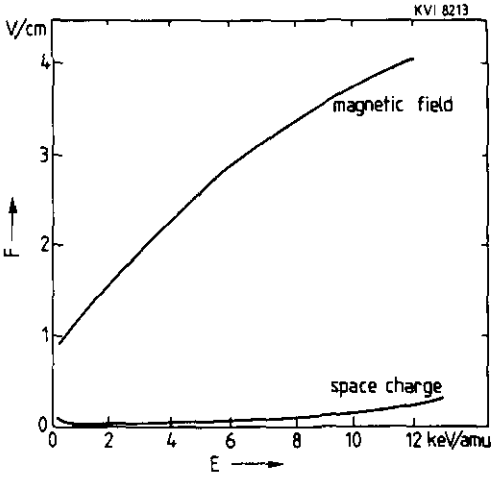

Figure 4. The electric field F due to the space charge of the ion beam and to the movement of the ions in the uncompensated magnetic field inside the collision chamber (see text).

atomic hydrogen this cross section is only 10^{-18} to 10^{-17} cm^2 (cf table 4). To check whether there is an interfering fraction of metastable hydrogen in the target beam we have applied electric fields up to 600 V cm^{-1} across the target beam to Stark mix the H(2s) and H(2p) states and to induce the related Lyman-α radiation at 121.6 nm. The highest field is more than strong enough to fully quench the H(2s) state (477 V cm^{-1} according to Risley *et al* 1978). We did not observe any signal above the background noise of the photon detection system. Taking the target flow and the overall sensitivity (counts per emitted photon) of the detection system into account this implies that the fraction of metastable H(2s) in the target beam is less than 10^{-9}. Therefore capture from metastables does not contribute to our experimental results.

2.3.5. Absolute errors. The absolute systematic errors are due to uncertainties in the absolute sensitivity calibration of the monochromators and the absolute target density. The error in the absolute sensitivity calibration is 15% for the visible light monochromator and 25% for the ultraviolet spectrometers (Kadota *et al* 1982). When using the ratio of the cross sections for Balmer-β excitation due to electron impact on H and H_2, respectively, the error in the determination of the target density becomes 17% (Čirič *et al* 1985). However using the constant gas flow method as described by Walker and St John (1974) the latter error may be reduced to 10% (Hoekstra 1990). Summing these errors quadratically yields an error of 20% for the He II ($n=4\rightarrow n=3$) emission cross section and of 30% for the other emission lines. However, from the comparison of the sum of all Lyman transitions Σ_n ($np\rightarrow 1s$) with the difference of the total charge transfer cross section σ_{tot} and the measured $He^+(2s)$ population $\sigma(2s)$ (taken from Shah and Gilbody 1978) it is possible to get a better idea of the actual absolute error in our measurements of the He II ($np\rightarrow 1s$) radiation. The above mentioned quantities are directly related by

$$\sigma_{tot}-\sigma(2s)=\sum_n (np\rightarrow 1s). \tag{6}$$

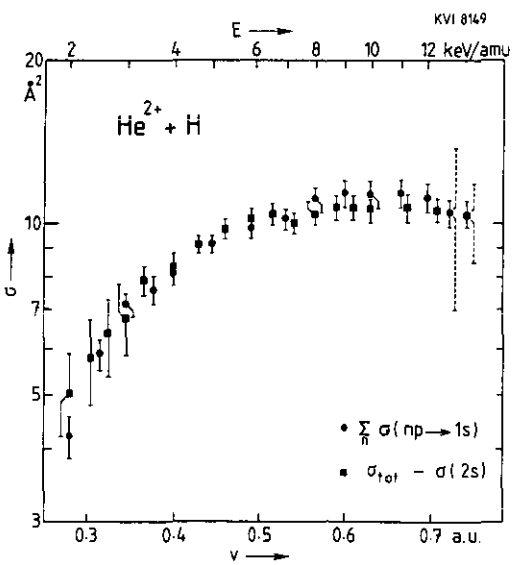

Figure 5. Comparison between our Σ_n He II ($np\rightarrow 1s$) results and the $\sigma_{tot}-\sigma(2s)$ values of Shah and Gilbody (1978). The full error bars are the relative errors and the broken error bars (shown only at the highest velocity point) give the absolute systematic errors.

This can be seen (cf figure 2) by realizing that each capture process will eventually lead either to a He II (np→1s) or a He II (np→2s) transition. The comparison between our Σ_n (n_p→1s) results and the $\sigma_{tot}-\sigma(2s)$ values of Shah and Gilbody (1978) is shown in figure 5. From this figure it can be seen that there is excellent agreement between both sets of measurements and therefore we feel confident to state that our absolute error is as large as the one of Shah and Gilbody (1978), namely 15%. Since Σ_n (np→1s) is for more than 95% due to the He II (2p→1s) emission, we assume for this transition the absolute error to be 15%. In combination with the relative wavelength dependent sensitivity of the spectrometer this yields absolute errors of 18% and 20% for the He II (3p→1s) and He II (4p→1s) transitions respectively.

Finally, with respect to possible systematic errors, it has to be remarked that some measurements were repeated with $^3He^{2+}$ to check the presence of impurity ions with the same charge to mass ratio (e.g. H_2^+ or C^{6+}) as He^{2+}. No systematic difference in the results was observed. Furthermore the fraction of He^+ ions in the primary beam (produced in charge transfer processes in the beam line after the last selecting magnet) is small, $\ll 1\%$.

3. Comparison of experiment and theory

Being the simplest asymmetric one-electron collision system, charge transfer in relatively slow He^{2+}-H collisions ($E < 15$ keV amu^{-1}) has been studied extensively by molecular oribital (MO) (e.g. Winter and Hatton 1980, Kimura and Thorson 1981, Errea *et al* 1987), atomic orbital (AO) (e.g. Bransden *et al* 1983, Fritsch 1988, Shingal and Lin 1989) and other expansion methods (e.g. the Hylleraas expansions of Lüdde and Dreizler (1982)). Regarding the total electron capture cross sections and the ones for the dominant capture channel, $He^+(2p)$, there is excellent agreement (10–15%) between the different sets of calculated cross sections. Therefore in section 3.1 we will compare our data for electron capture into $He^+(2p)$ with only one of them, namely the AO results of Fritsch (1988). For the minor channels (states with $n > 2$) discussed in sections 3.2 and 3.3 the number of theoretical results is so much smaller that a comparison can be made with all of them separately. However, the emphasis will again be on comparing the experimental data with the AO results of Fritsch (1988). These calculations are the most extended; they make use of a basis set of not less than 91 orbitals. This basis set includes all He^+ states with $n \leq 7$, the H states with $n = 1$ and 2 and the $n = 2$ states of the united atom. Since only a small fraction of the results has been published, the results relevant for comparison with our experimental data are presented in table 4. Furthermore, as will be shown in the next sections, the cross sections given in table 4 combined with the experimental data may be regarded as the benchmark ones for the He^{2+}-H collision system.

3.1. Capture into the dominant $He^+(n=2)$ level

The emission cross sections for the He II (2p→1s) transition, which are directly related to the dominant $He^+(2p)$ populations (cf figure 2), are shown in figure 6. It is seen that there is excellent agreement between experiment and theory. At impact velocities below 0.4 au our results (see also Hoekstra *et al* 1989) start to fall below the results of Čirič *et al* (1985). The difference now observed between theory and their results is due to the fact that in figure 6 we have chosen to present their uncorrected cross

Table 4. AO results for electron capture in He^{2+}–H collisions (Fritsch 1988). The n level cross sections are given in 10^{-16} cm^2. The nl state selective cross sections are given as the fraction of the n level cross sections.

			l values				
E (keV amu^{-1})	n	$\sigma(n)$	0	1	2	3	4
1.0	2	2.30	0.246	0.754			
	3	0.091	0.047	0.183	0.770		
	4	0.0045	0.052	0.150	0.264	0.534	
	5	0.0014	0.081	0.115	0.118	0.426	0.260
1.7	2	4.85	0.235	0.765			
	3	0.20	0.105	0.478	0.417		
	4	0.021	0.127	0.074	0.388	0.412	
	5	0.011	0.070	0.191	0.273	0.286	0.180
2.5	2	7.10	0.206	0.794			
	3	0.35	0.198	0.556	0.246		
	4	0.051	0.129	0.218	0.319	0.334	
	5	0.017	0.200	0.177	0.169	0.266	0.188
3.5	2	8.92	0.198	0.802			
	3	0.47	0.212	0.559	0.229		
	4	0.043	0.223	0.323	0.188	0.266	
	5	0.022	0.172	0.155	0.249	0.305	0.119
5.0	2	10.9	0.196	0.804			
	3	0.66	0.206	0.535	0.259		
	4	0.060	0.134	0.345	0.356	0.165	
	5	0.024	0.130	0.140	0.391	0.267	0.072
7.5	2	11.9	0.192	0.808			
	3	0.80	0.166	0.412	0.422		
	4	0.10	0.174	0.435	0.219	0.172	
	5	0.033	0.106	0.259	0.339	0.202	0.094
10.0	2	12.3	0.186	0.814			
	3	0.82	0.137	0.365	0.498		
	4	0.12	0.139	0.388	0.231	0.243	
	5	0.043	0.080	0.373	0.196	0.216	0.135
12.5	2	12.1	0.176	0.824			
	3	0.87	0.139	0.408	0.453		
	4	0.16	0.131	0.352	0.287	0.210	
	5	0.055	0.077	0.398	0.224	0.231	0.070
16.0	2	11.1	0.166	0.834			
	3	1.04	0.196	0.480	0.324		
	4	0.22	0.161	0.462	0.257	0.120	
	5	0.080	0.121	0.492	0.216	0.142	0.029

sections instead of the ones (over-)corrected for possible anisotropy of the photon emission (they applied the formulae for transitions in a singlet system instead of the ones for a doublet system like He II). Theoretical emission cross sections for observation of the emitted radiation perpendicular to the ion beam have been included in figure 6. They have been evaluated as described in appendix A from $He^+(2pm)$ cross sections (Fritsch 1988). It is seen that the influence of the anisotropy of the photon emission is small regarding cross sections determined from measurements under 90° (see also section 2.3.2).

The status of theoretical and experimental electron capture cross sections for the $He^+(2s)$ channel is shown in figure 7. We only show results of theoretical work that

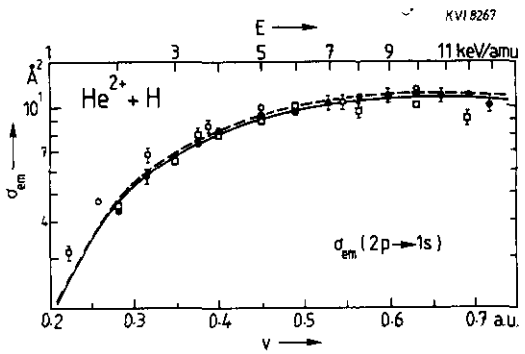

Figure 6. Emission cross sections for the He II (2p → 1s) transition. Theory: ——, - - -, AO results (Fritsch 1988); which are respectively uncorrected and corrected for polarization effects; Experiment: ○, Čirič *et al* (1985); □, Čirič *et al* (1988); ●, this work. Only relative errors are shown.

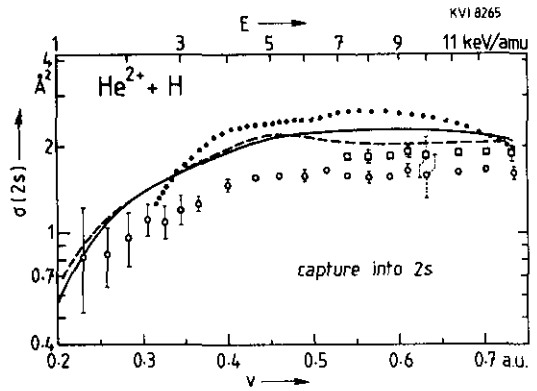

Figure 7. Population of the $He^+(2s)$ state. Theory: ——, Fritsch (1988); - - -, Errea *et al* (1987); · · · ·, Bransden and Noble (1981); Experiment: ○, □, Shah and Gilbody (1978) respectively uncorrected and corrected for polarization effects (see text). The full error bars are the relative errors and the broken error bars indicate the absolute systematic errors.

presented their cross sections in tabular form at a considerable number of impact energies. In the energy range of 3–13 keV amu^{-1} all theoretical treatments (also the ones not shown: Winter and Hatton 1980, Kimura and Thorson 1980, Bransden *et al* 1983, Winter 1988, Shingal and Lin 1989) predict an almost constant cross section being slightly larger than 2 Å^2, whereas the experimental results of Shah and Gilbody (1978) are approximately constant at a level of 1.6 Å^2. In this energy range the data (not shown) of Bayfield and Khayrallah (1975) exhibit a different energy dependence; they increase smoothly from 0.86 Å^2 at 3 keV amu^{-1} to 2.3 Å^2 at 13.75 keV amu^{-1}. In the context of the generally good agreement between theory and experiment for electron capture in other even less dominantly populated states (sections 3.2 and 3.3), the difference for the $He^+(2s)$ cross sections is somewhat surprising. To some extent the difference may be explained by polarization effects. The population of the metastable $He^+(2s)$ state has namely been measured by electric field quenching of these metastables and by detecting the resulting emission perpendicularly to the ion beam. The $He^+(2s)$ states are populated in a field free region and therefore, if the electric field is strong enough, the radiation can be fully polarized, $\Pi = -1$ (Harbich *et al* 1989). Due to this

the measured cross sections will be too small and need to be corrected by a factor of 1.33, cf equation (A.4). This would cover the gap between experiment and theory. However, from the strength of the electric field actually applied by Shah and Gilbody (1978) we estimate Π to be ~ -0.45 and in that case their data should be increased by only 15%, which has been done for some points presented in figure 7. It should be noted that our value of 15% is in accordance with the estimate of 10% made by Shah and Gilbody (1976) in a publication in which they re-evaluated their first series of measurements of this type (Shah and Gilbody 1974). Including the proposed correction the difference between theory and experiment becomes acceptable, although the situation is not totally satisfactory.

3.2. Capture into the semi-dominant $He^+(n=3)$ level

Figure 8 shows the emission cross sections for the He II (3p→1s) transition. It is seen that there is good agreement with previous measurements and with the extended AO calculations of Fritsch (1988), although the local minimum at $v = 0.6$ au is not apparent in our data. The smaller scale AO calculations by Bransden *et al* (1983) and the unitarized distorted-wave approximation (UDWA) calculations of Ryufuku (1982) clearly underestimate the cross sections. The more recent AO calculations by Shingal and Lin (1989) (not shown) are in fair agreement with the experiments, as estimated from the graphical presentation of their results.

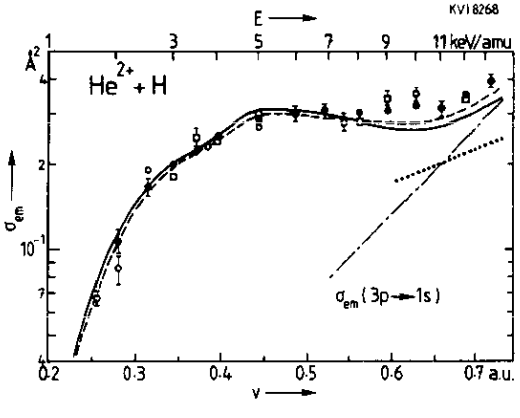

Figure 8. Emission cross sections for the He II (3p→1s) transition. Experiment and theory as figure 6 plus theoretical results of Bransden *et al* (1983) (— - —) and Ryufuku (1982) (· · · ·).

The small cross sections for capture into $He^+(4s)$ and $He^+(4d)$ (table 3) and the unfavourable branching ratios for decay from these states to $He^+(3p)$ imply that the He II (3p→1s) emission cross sections are directly related to the capture cross sections $\sigma(3p)$ by the 3p→1s branching ratio of 0.88 (figure 2). In figure 9 we present the summed cross sections for electron capture into $He^+(3s)$ and $He^+(3d)$, $\sigma(3s+3d)$, which are extracted from the He II ($n=3 \rightarrow n=2$) emission cross sections by

$$\sigma(3s+3d) = \sigma_{em}(n=3 \rightarrow n=2) - (0.12/0.88)\sigma_{em}(3p \rightarrow 1s). \tag{7}$$

Comparing theory and experiment the same level of agreement as for the 3p results is found for $\sigma(3s+3d)$ cross sections. Although there is a considerable difference in

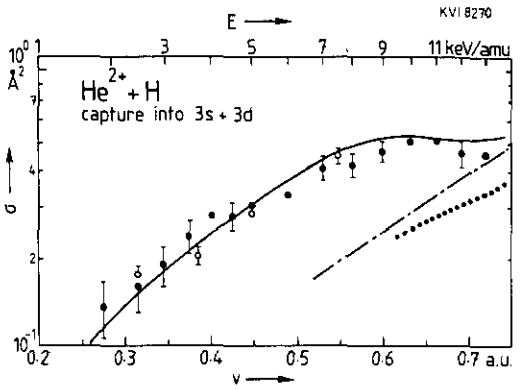

Figure 9. Cross sections for electron capture into $He^+(3s)$ plus $He^+(3d)$. Experiment and theory as in figure 8.

the lifetimes of the 3s and 3d states the deconvolution technique described in section 2.2 cannot be exploited. This is due to the long observation length of the Seya–Namioka spectrometer which covers approximately half of the total distance between the collimating diaphragm and the Faraday cup (see figure 1). Comparing figures 8 and 9 we see that at the higher impact velocities the data for 3p fall above the AO predictions whereas the summed 3s and 3d ones are slightly below theory. This might hint at a somewhat stronger relative population of the 3p state.

3.3. Capture into the non-dominant $He^+(n = 4)$ level

The cross sections measured for the emission lines related to the $He^+(n = 4)$ level, He II (4p → 1s) and He II ($n = 4 \rightarrow n = 3$), are shown in figures 10 and 11 together with the AO and UDWA results of Fritsch (1988) and Ryufuku (1982), respectively. Whereas the AO results predict some structures in the cross sections, the experimental data

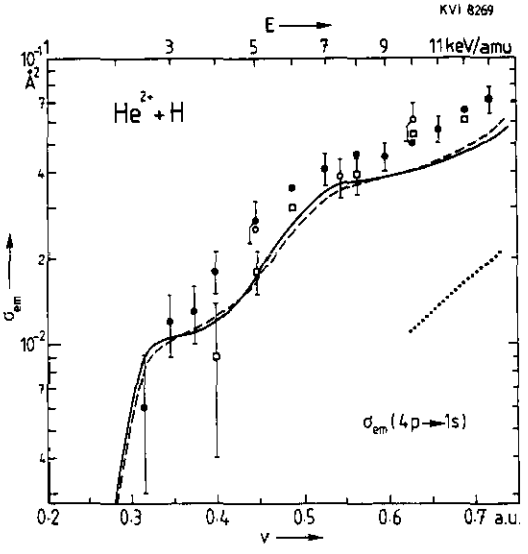

Figure 10. Emission cross sections for the He II (4p → 1s) transition. Experiment and theory as figure 6 plus theoretical results of Ryufuku (1982) (· · · · ·).

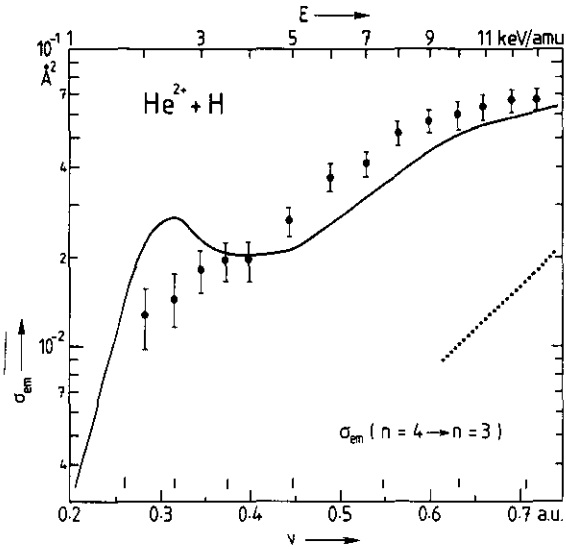

Figure 11. Emission cross sections for the He II ($n = 4 \rightarrow n = 3$) transition. Theory: ——, AO results (Fritsch 1988); · · · ·, UDWA results (Ryufuku 1982). Experiment: ●, this work. Only relative errors are shown.

increase smoothly with increasing impact velocity. To us there is no clear reason to explain the energy-dependent structures in the population of these highly excited states (strongly endothermic capture reactions). Since the relative numerical uncertainty in the AO calculations is rather small, the structure might be due to the fact that the basis set, although very large already, is still not yet sufficiently large. However, considering the fact that the cross sections are more than two orders of magnitude smaller than the dominant one for capture into $He^+(2p)$, charge transfer into these minor channels seems to be fairly well described by the AO treatment of Fritsch (1988). Comparison of the data with the UDWA results (Ryufuku 1982) demonstrates the well known inappropriateness of this treatment at $v < 1$ au for calculating capture into non-dominantly populated high-lying states.

The state-selective electron capture cross sections for the 4s, 4d and 4f states deduced from the He II ($n = 4 \rightarrow n = 3$) emission profiles by means of the deconvolution technique (section 2.2) are shown in figure 12. The results increase more or less smoothly with increasing velocity. Especially in $\sigma(4d)$ and $\sigma(4f)$ of the AO calculations there are the pronounced structures that led to the structure in the He II ($n = 4 \rightarrow n = 3$) cross sections discussed above. It should be noted that our experimental 4s cross sections are enhanced by some factor of two due to $5g \rightarrow 4f \rightarrow 3d$ cascades. Notwithstanding that the 5g state does not decay directly to the 4s state it does contribute to $\sigma(4s)$ because the effective lifetime of this cascade series is close to the one of the 4s state (cf figure 2). Therefore the 5g and the 4s contributions to the He II ($n = 4 \rightarrow n = 3$) line cannot be resolved by our lifetime based deconvolution technique. The effect of the cascades originating from 5g on the 4s cross sections is amplified by the fact that the branching ratios for the subsequent cascade steps are 1, whereas the branching ratio for the $4s \rightarrow 3p$ is only 0.42, see figure 1.

For the interpretation of spectra observed on large tokamaks it is important to know electron capture cross sections for high-n levels. A common way to estimate

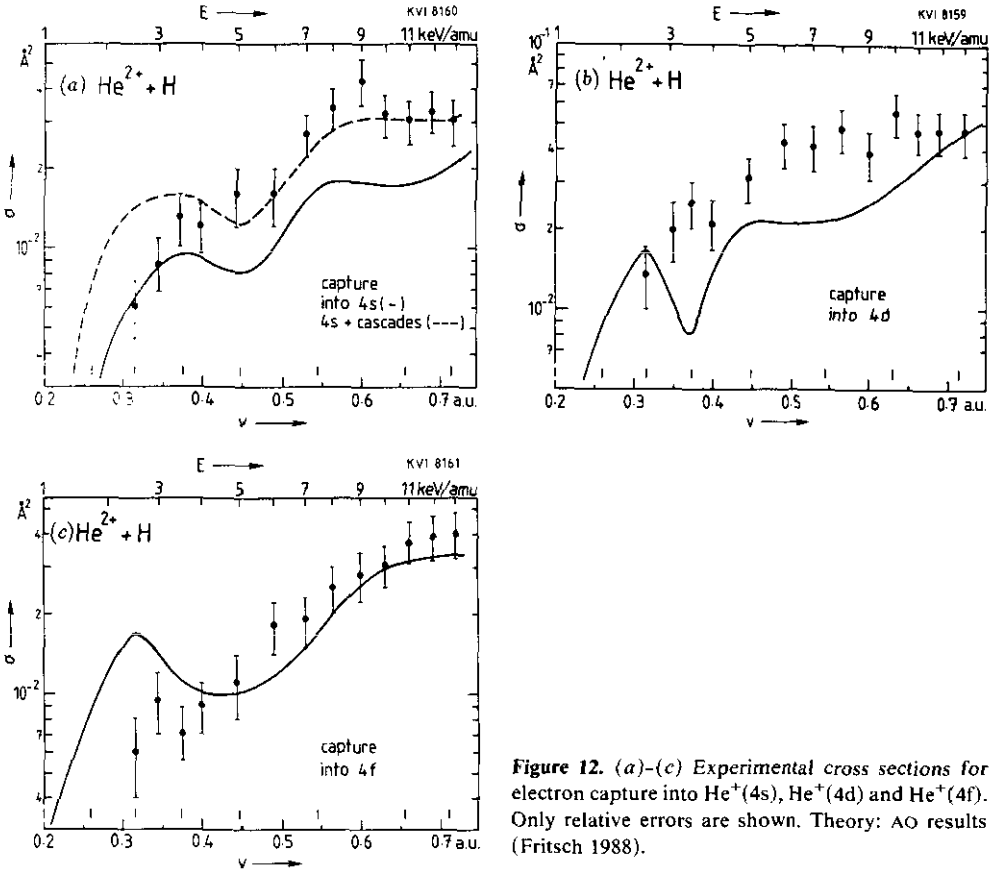

Figure 12. *(a)-(c) Experimental cross sections for* electron capture into $He^+(4s)$, $He^+(4d)$ and $He^+(4f)$. Only relative errors are shown. Theory: AO results (Fritsch 1988).

them is using an $n^{-\gamma}$ scaling, with $\gamma = 3$ (see e.g. Spence and Summers 1986). Since $\gamma = 3$ arises in high energy approximations based on the available density of excited states in the ion, it is realized that at lower energies the cross sections for high-n states will decrease more rapidly with increasing n value (see von Hellermann *et al* 1991). An impression of the validity range of the n^{-3} scaling may be obtained from our $n = 3$ and 4 cross sections. The $n = 3$ cross sections are found from summing the He II $(n = 3 \rightarrow n = 2)$ and He II $(3p \rightarrow 1s)$ emission cross sections and the $n = 4$ ones are determined by summing the 4s, 4d and 4f capture cross sections and the He II $(4p \rightarrow 1s)$ emission cross section divided by its branching ratio of 0.84. For the 4s cross sections we have taken half of the values given in table 3 to account for the contributions of the 5g cascades. The values of γ calculated in this way are given in table 5. From this table it is seen that γ is indeed much larger than 3. Extrapolating these values to higher impact energies we do not expect that $\gamma = 3$ will be reached at energies below 25 keV amu^{-1} ($v = 1$ au).

Table 5. The scaling power γ ($n^{-\gamma}$), deduced from $\sigma(n = 3)$ and $\sigma(n = 4)$.

E (keV amu^{-1})	2.5	4	6	8	10	13
v (au)	0.32	0.4	0.49	0.57	0.63	0.72
γ	8.5	7.9	6.4	5.9	5.7	5.4

4. Conclusions

In this paper on He^{2+}–H collisions we have shown that it is possible to determine the separate $He^{+}(4l)$ contributions to the spectroscopically unresolved He II ($n=4\rightarrow n=3$) line emission. This has been done by a deconvolution method based on the different lifetimes of the $4l$ states. So in the energy range of 2–13 keV amu^{-1} state-selective cross sections for electron capture into non-dominantly populated high-n states could be determined. Not only in this energy range are cross sections relevant for fusion plasma diagnostics but also at higher energies. Therefore we have extended this kind of measurement up to energies of 125 keV amu^{-1} (Frieling *et al* 1991).

Considering the small magnitude of the $He^{+}(4l)$ electron capture cross sections it may be concluded that there is generally good agreement with the most extended atomic orbital calculations by Fritsch (1988). However, the structures in the theoretical cross sections for capture into these non-dominantly populated $n=4$ states are not observed experimentally. We have also measured absolute emission cross sections for transitions originating from the dominantly and semi-dominantly populated states, 2p and $n=3$ respectively. From all these cross sections an almost complete picture of state-selective charge transfer in collisions of He^{2+} with atomic hydrogen has emerged, especially in combination with the results of the AO calculations mentioned above. The present set of data for electron capture in collisions of He^{2+} with H at impact energies of 2–13 keV amu^{-1} may be regarded as a benchmark set against which future calculations may be tested.

Acknowledgments

We would like to thank Dr W Fritsch of the Hahn Meitner Institute (Berlin) for providing us with all the numerical results of his AO calculations and performing some extra calculations at energies in the range of 2–4 keV amu^{-1}. Furthermore we want to thank J Sijbring and J Eilander for their technical support. This work is part of the research program of the 'Stichting voor Fundamenteel Onderzoek der Materie' (FOM), which is financially supported by the 'Stichting voor Nederlands Wetenschappelijk Onderzoek' (NWO). Via an article 14 contract with JET (Culham, England) the work is also part of the research program of the association agreement between FOM and EURATOM with financial support by NWO.

Appendix A. Polarization effects

The dipole radiation emitted by an atom or ion is polarized. The degree of polarization is defined as

$$\Pi(\theta)=\frac{I_{\parallel}(\theta)-I_{\perp}(\theta)}{I_{\parallel}(\theta)+I_{\perp}(\theta)} \tag{A.1}$$

where $I_{\parallel}(\theta)$ and $I_{\perp}(\theta)$ are the light intensities, emitted at an angle θ with respect to the ion beam, polarized respectively in the plane and perpendicular to the plane defined by the ion beam and the line of observation. The polarization affects the accuracy of our results in two ways:

(i) The radiation will be emitted anisotropically. The intensity of light emitted at an angle θ is related to the polarization Π at 90° by (see e.g. Moiseiwitsch and Smith 1969 and references therein)

$$I(\theta) = I(90°)(1 - \Pi \cos^2 \theta). \tag{A.2}$$

The correction factor $P_1(\theta)$ by which the experimental results should be multiplied to correct for the anisotropy of the emitted radiation is

$$P_1(\theta) = \frac{3 - \Pi}{3(1 - \Pi \cos^2 \theta)}. \tag{A.3}$$

At the so-called *magic angle* of observation of 54.7°, $\cos^2 \theta = \frac{1}{3}$, and therefore P_1 is 1 and independent of Π. for the observation angle of 90° the correction factor is

$$P_1(\theta) = 1 - \tfrac{1}{3}\Pi. \tag{A.4}$$

Since $|\Pi| \leq 1$ the error due to neglecting polarization can be at most 33%.

(ii) The monochromators may have different sensitivities $K_\parallel(\lambda)$ and $K_\perp(\lambda)$ for parallel and perpendicularly polarized light respectively. Influences of these different sensitivities can be eliminated by tilting the monochromator around the observation axis in such a way that the entrance slit is inclined under 45° with the ion beam (Clout and Heddle 1969). This has been done for both our VUV monochromators. The monochromator for visible light is not tilted, to allow measuring of emission profiles along the ion beam axis. The correction factor P_2 for an instrumental effect is given by (Wolterbeek Muller and de Heer 1970)

$$P_2 = \frac{(B+1)(C+1)}{2(BC+1)} \tag{A.5}$$

with

$$B = \frac{K_\parallel(\lambda)}{K_\perp(\lambda)} \qquad C = \frac{I_\parallel}{I_\perp} = \frac{1+\Pi}{1-\Pi}. \tag{A.6}$$

At the wavelength of the He II ($n = 4 \rightarrow n = 3$) transition, 468.6 nm, the sensitivity ratio B is 0.67. This ratio has been measured by means of a quartz-iodine lamp (Stair *et al* 1963) and a set of polarization filters. The total polarization correction factors P_1 and P_2 are shown in figure A1 as a function of Π together with the total polarization factor P, which is the product of P_1 and P_2. It can be seen that P_1 and P_2 have an opposite Π-dependence and almost cancel each other. Therefore the total correction factor is close to one, with a maximum deviation of 10%. However realizing that the He II ($n = 4 \rightarrow n = 3$) transition is due to different $4l \rightarrow 3l'$ transitions and that not for all transitions can the maximum polarization $|\Pi| = 1$ be reached (Percival and Seaton 1958) the error due to neglecting the polarization is probably much smaller than the 10% mentioned above. So to get a realistic impression of the maximum error due to neglect of polarization it is important to know Π_{min} and Π_{max}, i.e. the minimum and maximum value of Π theoretically possible.

In the *LS* coupling scheme the initial and final levels of a transition can be characterized by $LSJM_j$ and $L'S'J'M_j'$, with L, S, J and M_j respectively the orbital, spin, total angular momentum and total magnetic quantum number. We will assume spin conservation which means $S' = S$ and a nuclear spin of 0. For observation under 90° it has been shown (Sobelmann 1975), that for a $LSJM_j \rightarrow L'SJ'M_j'$ transition the intensity of light polarized parallel and perpendicular to the ion beam is due to

respectively $\Delta M_j = 0$ and $\Delta M_j = \pm 1$ transitions (the ion beam axis is taken as the z axis). Since we only measure transitions between specific LS and $L'S$ states the light intensities polarized parallel, $I_{\parallel}(LS \to L'S)$ and perpendicular, $I_{\perp}(LS \to L'S)$ to the ion beam are given by:

$$I_{\parallel}(LS \to L'S) = C \sum_J \left\{ \sum_{J'} \left\{ \frac{\mathcal{S}(LSJ \to L'SJ')}{\sum_{J'} \mathcal{S}(LSJ \to L'SJ')} \sum_{M_j} \sigma_{LSJM_j}(2J+1) \begin{pmatrix} J' & 1 & J \\ M_j & 0 & -M_j \end{pmatrix}^2 \right\} \right\} \tag{A.7}$$

$$I_{\perp}(LS \to L'S) = \tfrac{1}{2} C \sum_J \left\{ \sum_{J'} \left\{ \frac{\mathcal{S}(LSJ \to L'SJ')}{\sum_{J'} \mathcal{S}(LSJ \to L'SJ')} \sum_{M_j} \sigma_{LSJM_j}(2J+1) \times \left[\begin{pmatrix} J' & 1 & J \\ M_j - 1 & 1 & -M_j \end{pmatrix}^2 + \begin{pmatrix} J' & 1 & J \\ M_j + 1 & -1 & -M_j \end{pmatrix}^2 \right] \right\} \right\} \tag{A.8}$$

where C is a constant depending only on L and L', $\mathcal{S}(LSJ \to L'SJ')$ is the line strength and σ_{LSJM_j} is the population of the $LSJM_j$ state. The line strength depends on J and J' as follows:

$$\mathcal{S}(LSJ \to L'SJ') \propto (2J+1)(2J'+1) \begin{Bmatrix} L & J & S \\ J' & L' & 1 \end{Bmatrix}^2. \tag{A.9}$$

The σ_{LSJM_j} distribution necessary for calculating these light intensities can be found by coupling the LM_L states with the SS_Z spin states. Assuming an equal population of the S_Z states and no dependence on the experimental conditions of the distribution over the J states within one L multiplet (this is not unrealistic since the energy splitting is very small) the final σ_{LSJM_j} distribution is given by

$$\sigma_{LSJM_j} = \frac{1}{(2S+1)} \sum_{M_L + S_Z} |\langle LM_L SS_Z | JM_j \rangle|^2 \sigma_{LM_L}. \tag{A.10}$$

We have performed the stepwise calculations described above for some relevant configurations. The results are given in table A.1 where we have used the relation $\sigma_{nlm} = \sigma_{nl-m}$ to eliminate values of $m_2 < 0$ and skipped the subscripts *nl*. Table A.1 also includes the minimum and maximum values of the polarization Π_{min} and Π_{max}, respectively. Combining these extreme values of the polarization with figure A1 it is seen that for the He II ($n = 4 \to n = 3$) transition the error due to neglecting polarization is always smaller than 5%.

Table A.1. Formula for the polarization Π and its maximum and minimum values Π_{max} and Π_{min} respectively for doublet transitions. Π is 0 for all transitions from states with $L = 0$.

Initial state	Final state	Π	Π_{min}	Π_{max}
p P°	s S	$\dfrac{3\sigma_0 - 3\sigma_1}{7\sigma_0 + 11\sigma_1}$	−0.27	0.43
d D	p P°	$\dfrac{3\sigma_0 + 3\sigma_1 - 6\sigma_2}{11\sigma_0 + 21\sigma_1 + 18\sigma_2}$	−0.33	0.27
f F°	d D	$\dfrac{258\sigma_0 + 387\sigma_1 - 645\sigma_3}{576\sigma_0 + 1109\sigma_1 + 980\sigma_2 + 765\sigma_3}$	−0.85	0.45

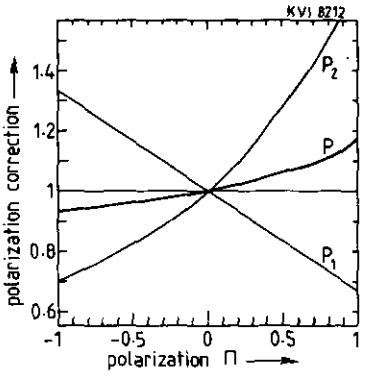

Figure A1. Polarization correction factors P_1 (anisotropy of the radiation) and P_2 (instrumental effects) for the He II ($n=4 \rightarrow n=3$) transition at 468.6 nm as a function of the polarization Π. The total correction factor P given by $P_1 \times P_2$ is also shown.

Appendix B. Stark effect

Electric fields cause Stark mixing of field-free eigenstates. This mixing can have considerable impact on the lifetimes and transition probabilities of the atomic states (e.g. Bethe and Salpeter 1957, Havener *et al* 1986, Van Zyl *et al* 1988). Accurate knowledge of lifetimes and branching ratios is needed to deduce electron capture cross sections from the He^+ ($n=4 \rightarrow n=3$) line emission. Therefore it is important to know the influence of electric fields on the lifetimes and branching ratios of the $He^+(4l)$ states. In the following we will briefly outline the formalism (for details see Bethe and Salpeter 1957) and show the results for the $He^+(4l)$ states.

The Hamiltonian $\boldsymbol{H}$ of a hydrogen-like ion $A^{(z-1)+}$ (nuclear charge Z) in a homogeneous external electric field F (parallel to the z axis) is given by (in SI units)

$$\boldsymbol{H} = \underbrace{\frac{\boldsymbol{p}^2}{2m} - \frac{Ze^2}{4\pi\varepsilon_0 r}}_{\boldsymbol{H}_0} \underbrace{- \frac{\boldsymbol{p}^4}{8m^2c^2} - \frac{Ze^2}{8\pi\varepsilon_0 m^2 c^2 r^3}(\boldsymbol{L}\cdot\boldsymbol{s})}_{\boldsymbol{H}_1} \underbrace{+ ezF}_{\boldsymbol{H}_2} \tag{B.1}$$

where $\boldsymbol{H}_0$, $\boldsymbol{H}_1$ and $\boldsymbol{H}_2$ respectively represent the kinetic plus potential energy, the fine-structure splitting and the 'linear Stark effect', $\boldsymbol{p}$ the momentum, m the reduced mass of the electron, e the electronic charge, c the speed of light and r the distance of the electron to the nucleus. If $\boldsymbol{H}_2$ is negligible with respect to the fine-structure-splitting term $\boldsymbol{H}_1$, the Schrödinger equation can be solved exactly yielding the well known field-free eigenfunctions $|nljm_j\rangle$ with their energy eigenvalues.

For the cases that $\boldsymbol{H}_2$ cannot be neglected we shall consider only 'small' fields such that the energy splitting due to $\boldsymbol{H}_2$ is considerably smaller than the energy difference between adjacent n-levels (E_0). Therefore expanding an eigenfunction ϕ of $\boldsymbol{H}$ in field-free eigenfunctions (i.e. mixing), only eigenfunctions with the same n-value have to be used:

$$\phi = \sum_{j,l=j\pm 1/2,m_j} a_{nljm_j}(F)|nljm_j\rangle \tag{B.2}$$

and

$$\sum_{j,l=j\pm 1/2,m_j} |a_{nljm_j}(F)|^2 = 1.$$

The following well known eigenvalue problem has to be solved:

$$\sum_{j,l=j\pm1/2,m_j} a_{nljm_j}(F)\langle nljm_j|\boldsymbol{H}|nl'j'm_j'\rangle = Ea_{nl'j'm_j'}(F). \tag{B.3}$$

Taking the energy corresponding to $\boldsymbol{H}_0$ as zero-point energy, the non-zero matrix elements $\langle nljm_j|\boldsymbol{H}|nl'j'm_j'\rangle$ are given by (Lüders 1951)

$$\langle nljm_j|\boldsymbol{H}|nljm_j\rangle = -\tfrac{1}{2}mc^2\left(\frac{Z\alpha}{n}\right)^4\left(\frac{n}{j+\frac{1}{2}}-\frac{3}{4}\right) \tag{B.4a}$$

$$\langle nljm_j|\boldsymbol{H}|nl+1j+1m_j\rangle = 4\pi\varepsilon_0\frac{F\hbar^2}{Zme}\frac{3n[((j+1)^2-m_j^2)n^2-(l+1)^2]^{1/2}}{4(j+1)} \tag{B.4b}$$

$$\langle nljm_j|\boldsymbol{H}|nl+1jm_j\rangle = -4\pi\varepsilon_0\frac{F\hbar^2}{Zme}\frac{3nm_j[n^2-(l+1)^2]^{1/2}}{4j(j+1)} \qquad \text{with } l=j-\tfrac{1}{2} \tag{B.4c}$$

where α is the fine structure constant $(137.037)^{-1}$. From these formulae it is clear that only m_j is preserved; l and j are no longer good quantum numbers. Each value of m_j corresponds to $2(n-m_j)$ different energy eigenvalues, $E^i_{nm_j}$, and eigenfunctions, $\phi^i_{nm_j}$ $(i=1\ldots 2(n-m_j))$. A few corrections to the matrix elements on the main diagonal have to be made. In the first place the Lamb shift (see e.g. Bethe and Salpeter 1957) has to be added. Secondly a term $-\frac{1}{2}i\hbar\Gamma_{nl}$ has to be added to account phenomenologically for the radiative decay (see Havener *et al* 1986, Lévy 1984). Γ_{nl} is the transition rate to all lower states and equals the inverse lifetime τ^{-1} of a field-free eigenfunction with quantum numbers nl; the quantity $\hbar\Gamma_{nl}$ is the so-called radiation width. Through the imaginary terms, $-\frac{1}{2}i\hbar\Gamma_{nl}$, the eigenvalues $E^i_{nm_j}$ and the expansion coefficients $a^i_{nljm_j}$ become complex numbers. Because the time dependence of a state is related to $\exp(-iEt/\hbar)$, the real part of $E^i_{nm_j}$ is the binding energy, and twice the imaginary part of $E^i_{nm_j}$ gives the inverse lifetime of the state. To find the eigenvalues the Hamiltonian

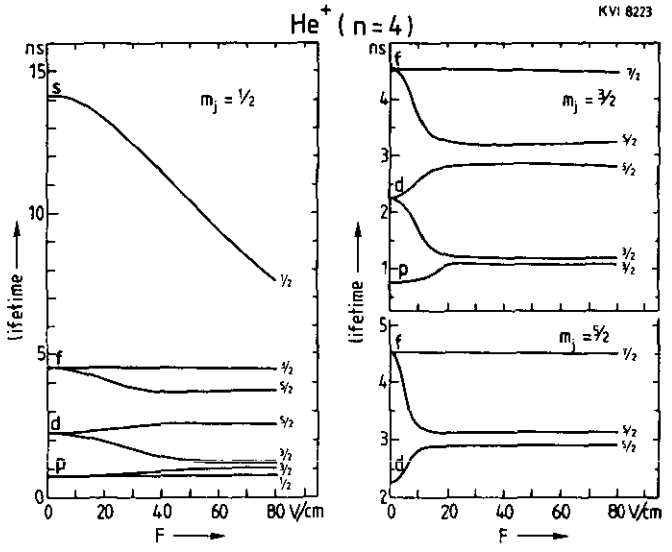

Figure B1. Lifetimes of $He^+(n=4)$ levels as a function of an electric field. The numbers on the right of each panel indicate the j values of the field free states of which the states have evolved. The l values of the field-free states are indicated on the left of each panel.

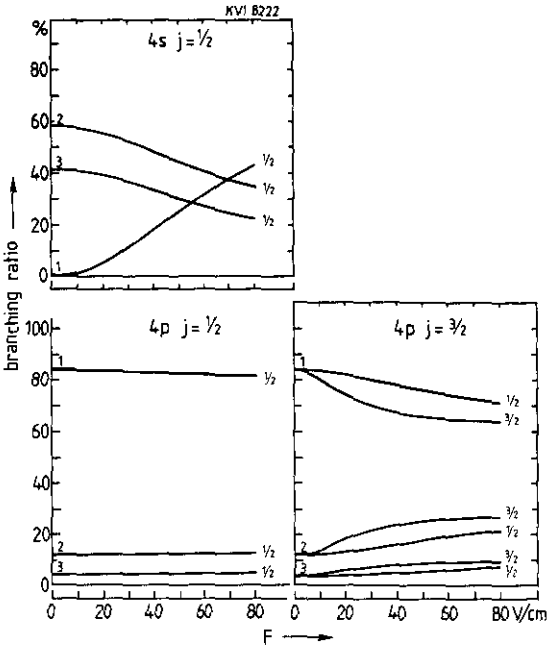

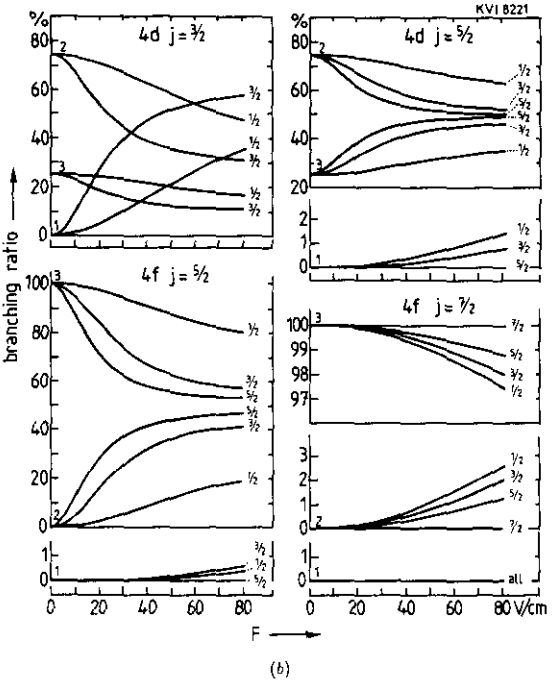

Figure B2. (*a*), (*b*) Branching ratios for $He^+(n=4)$ states. The numbers on the right side of the panels indicate the m_l values. The numbers directly on the right side of the left axis of the panels indicate the final n level of the transition.

matrix was diagonalized. This has been done by reducing the Hamiltonian matrix to a Hessenberg matrix and thereafter applying the so-called QR algorithm with origin shift (Young and Gregory 1973). In figure B1 we show the obtained lifetimes of the $He^+(n=4)$ states as a function of the applied electric field. From these figures it is seen that the lifetimes of the states evolving from the $4d(j=\frac{5}{2}$ and $m_j=\frac{5}{2})$ and the $4f(j=\frac{5}{2}$ and $m_j=\frac{5}{2})$ field-free states are the first ones to be influenced. The effect is already notable at fields as small as 2 V cm^{-1}. Therefore in our experiments we have to assure that the electric fields in the collision region are well below 2 V cm^{-1}, otherwise problems with lifetimes will arise.

It has been shown (Boorsma 1988, van Zyl *et al* 1988) that in an applied electric field the effective branching ratios $\mathcal{B}^{n'l'j'm_j'}_{nljm_j}$ of the $|nljm_j\rangle$ states are related to the field free branching ratios $\mathcal{B}^{n'l'j'm_j'}_{nljm_j}$ by

$$\mathcal{B}^{n'l'j'm_j'}_{nljm_j}=\sum_{ljm_j} B^{n'l'j'm_j'}_{nljm_j}\Gamma_{nl}\sum_i\sum_{i'}\left(\frac{a^i_{nljm_j}a^{i'*}_{nljm_j}(a^{-1})^i_{nljm_j}(a^{-1})^{i'*}_{nljm_j}}{i(E^i_{nm_j}-E^{i'*}_{nm_j})}\right). \tag{B.5}$$

Applying this formula the branching ratios of the $He^+(n=4)$ states in an electric field can be calculated. To check the reliability of our calculations we have calculated the branching ratios for $H(4s)$, which can be compared with calculations by van Zyl *et al* (1988). We found excellent agreement between our results (Hoekstra 1990) and their two-state calculations (mixing of states with the same j-value only) for electric fields up to 20 V cm^{-1}, at higher fields states with different j-values start to mix too.

Since it is not possible to resolve spectroscopically transitions originating from one specific nl state to different l' states within one lower-lying n' level, we present in figure B2(a) and (b) branching ratios summed over l'. It becomes clear from the figures that for electric fields below 2 V cm^{-1} there will be no problems with changing branching ratios, however increasing the field to higher values it is seen that especially the branching ratios of the 4d state with $j=\frac{3}{2}$ and of the 4f state with $j=\frac{5}{2}$ change rapidly.

References

Aumayr F, Fehringer M and Winter H 1984 *J. Phys. B: At. Mol. Phys.* **17** 4201

Bayfield J E and Khayrallah G A 1975 *Phys. Rev.* A **12** 869

Bethe H A and Salpeter E E 1957 *Quantum Mechanics of One- and Two-Electron Atoms* (Berlin: Springer)

Blanco S A, Falcón C A, Reinhold C O, Casaubón J I and Piacentini R D 1987 *J. Phys. B: At. Mol. Phys.* **20** 6295

Boileau A, von Hellermann M, Horton L D, Spence J and Summers H P 1989 *Plasma Phys. Controlled Fusion* **31** 779

Boorsma K 1988 *Stark effect in hydrogen-like atoms KVI internal report*

Bransden B H and Noble C J 1981 *J. Phys. B: At. Mol. Phys.* **14** 1849

Bransden B H, Noble C J and Chandler J 1983 *J. Phys. B: At. Mol. Phys.* **16** 4191

Čirič D, Dijkkamp D, Vlieg E and de Heer F J 1985 *J. Phys. B: At. Mol. Phys.* **18** 4745

Čirič D, Hoekstra R, de Heer F J and Morgenstern R 1988 *Electronic and Atomic Collisions* ed H B Gilbody, W R Newell, F H Read and A C H Smith (Amsterdam: North-Holland) p 655

Clout P N and Heddle D W O 1969 *J. Opt. Soc. Am.* **59** 715

Drentje A G 1985 *Nucl. Instrum. Methods* B **9** 526

Errea L F, Gómez-Llorente J M, Méndez L and Riera A 1987 *J. Phys. B: At. Mol. Phys.* **20** 6089

Fite W L, Smith A C H and Stebbings R F 1962 *Proc. R. Soc.* A **268** 340

Fonck R J, Darrow D S and Jähnig K P 1984 *Phys. Rev.* A **29** 3288

Frieling G J, Hoekstra R, Smulders E, Dickson W J, Zinoviev A N, Kuppens S J and de Heer F J 1991 *J. Phys. B: At. Mol. Opt. Phys.* submitted for publication

Fritsch W 1988 *Phys. Rev.* A **38** 2664 and private communication

Geller R and Jacquot B 1982 *Nucl. Instrum. Methods* **202** 399
Harbich W, Hippler R, Kleinpoppen H and Lutz H O 1989 *Phys. Rev.* A **39** 3388
Havener C C, Rouze N, Westerveld W B and Risley J S 1986 *Phys. Rev.* A **33** 276
Hoekstra R 1990 *Thesis* R U Groningen (available upon request)
Hoekstra R, de Heer F J and Morgenstern R 1991 *J. Phys. B: At. Mol. Opt. Phys.* to be submitted
Hoekstra R, Schlatmann A R, de Heer F J and Morgenstern R 1989 *J. Phys. B: At. Mol. Opt. Phys.* **22** L603
Janev R K and Winter H 1985 *Phys. Rep.* **117** 265
Kadota K, Dijkkamp D, van der Woude R L, de Boer A, Pan G Y and de Heer F J 1982 *J. Phys. B: At. Mol. Phys.* **15** 3275
Kimura M and Thorson W R 1981 *Phys. Rev.* A **24** 3019
Lévy L P 1984 *Phys. Rev.* A **29** 3189
Lüdde H J and Dreizler R M 1982 *J. Phys. B: At. Mol. Phys.* **15** 2713
Lüders G 1951 *Ann. Phys., Lpz.* **8** 301
Mathews J and Walker R L 1970 *Mathematical Methods of Physics* (Menlo Park, CA: Benjamin/Cummings)
Moiseiwitsch B L and Smith S J 1968 *Rev. Mod. Phys.* **40** 238
Nutt W L, McCullough R W, Brady K, Shah M B and Gilbody M B 1978 *J. Phys. B: At. Mol. Phys.* **11** 1457
Percival I C and Seaton M J 1958 *Phil. Trans. Soc.* A **251** 113
Risley J S, de Heer F J and Kerkdijk C B 1978 *J. Phys. B: At. Mol. Phys.* **11** 1759
Ryufuku H 1982 *Rep. JAERI-M-82-031*
Shah M B and Gilbody H B 1974 *J. Phys. B: At. Mol. Phys.* 7 630
—— 1976 *J. Phys. B: At. Mol. Phys.* **9** 1933
—— 1978 *J. Phys. B: At. Mol. Phys.* **11** 121
Shingal R and Lin C D 1989 *J. Phys. B: At. Mol. Opt. Phys.* **22** L445
Slevin J and Stirling W 1981 *Rev. Sci. Instrum.* **52** 1780
Sobelmann I I 1979 *Atomic Spectra and Radiative Transitions* (Berlin: Springer)
Spence J and Summers H P 1986 *J. Phys. B: At. Mol. Phys.* **19** 3749
Stair R, Schneider W E and Jackson J K 1963 *Appl. Opt.* **11** 1151
van Zyl B, van Zyl B K and Westerveld W B 1988 *Phys. Rev.* A **37** 4201
von Hellermann M, Mandl W, Summers H P, Boileau A, Hoekstra R, de Heer F J and Frieling G J 1991 *Plasma Phys. Controlled Fusions* in press
Walker J D Jr and St John R M 1974 *J. Chem. Phys.* **71** 2394
Winter T G 1988 *Phys. Rev.* A **37** 4656
Winter T G and Hatton G J 1980 *Phys. Rev.* A **21** 793
Wolterbeek Muller L and de Heer F J 1970 *Physica* **48** 345
Young D M and Gregory R T 1973 *A Survey of Numerical Mathematics* vol 2 (Reading, MA: Addison-Wesley)